A Multi-scale Modeling System: Developments, Applications and Critical Issues

Wei-Kuo Tao[1], Jiundar Chern[1,2], Robert Atlas[3], David Randall[4],
Xin Lin[2,6], Marat Khairoutdinov[4], Jui-Lin Li[5], Duane E. Waliser[5], Arthur Hou[6],
Christa Peters-Lidard[7], William Lau[1], and Joanne Simpson[1]

[1]*Laboratory for Atmospheres*
NASA/Goddard Space Flight Center
Greenbelt, MD 20771, USA

[2]*Goddard Earth Sciences and Technology Center*
University of Maryland, Baltimore County
Baltimore, MD

[3]*NOAA Atlantic Oceanographic and Meteorological Laboratory*
Miami FL 33149

[4]*Department of Atmospheric Science*
Colorado State University
Fort Collins, CO 80523

[5] *NASA/Jet Propulsion Laboratory-California Inst. of Technology*
Pasadena, CA 91109

[6]*Goddard Modeling Assimilation Office*
Greenbelt, MD 20771

[7]*Hydrological Sciences Branch*
Greenbelt, MD 20771

February 5, 2007

J. Geophy. Res.

---

[1] *Corresponding author address: Dr. Wei-Kuo Tao, Code 613.1, NASA Goddard Space Flight Center, Greenbelt, MD 20771, tao@agnes.gsfc.nasa.gov*

Abstract

A multi-scale modeling framework (MMF), which replaces the conventional cloud parameterizations with a cloud-resolving model (CRM) in each grid column of a GCM, constitutes a new and promising approach. The MMF can provide for global coverage and two-way interactions between the CRMs and their parent GCM. The GCM allows global coverage and the CRM allows explicit simulation of cloud processes and their interactions with radiation and surface processes.

A new MMF has been developed that is based the Goddard finite volume GCM (fvGCM) and the Goddard Cumulus Ensemble (GCE) model. This Goddard MMF produces many features that are similar to another MMF that was developed at Colorado State University (CSU), such as an improved surface precipitation pattern, better cloudiness, improved diurnal variability over both oceans and continents, and a stronger, propagating Madden-Julian oscillation (MJO) compared to their parent GCMs using conventional cloud parameterizations. Both MMFs also produce a precipitation bias in the western Pacific during Northern Hemisphere summer. However, there are also notable differences between two MMFs. For example, the CSU MMF simulates less rainfall over land than its parent GCM. This is why the CSU MMF simulated less overall global rainfall than its parent GCM. The Goddard MMF overestimates global rainfall because of its oceanic component. Some critical issues associated with the Goddard MMF are presented in this paper.

1. Introduction

The foremost challenge in parameterizing convective clouds and cloud systems in large-scale models are the many coupled, dynamical and physical processes that interact over a wide range of scales, from microphysical scales to the synoptic and planetary scales. This makes the comprehension and representation of convective clouds and cloud systems one of the most complex scientific problems in earth science. During the past decade, the GEWEX Cloud System Study (GCSS) has pioneered the use of single-column models (SCMs) and cloud-resolving models (CRMs; also called cloud-system resolving models or CSRMs) for the evaluation of the cloud and radiation parameterizations in general circulation models (GCMs; e.g., GCSS 1993). These activities have uncovered many systematic biases in the radiation and cloud parameterizations of GCMs and have lead to the development of new schemes (e.g., Pincus *et al.* 2003; Zhang 2002). Comparisons between SCMs and CRMs using the same large-scale forcing derived from field campaigns have demonstrated that CRMs are superior to SCMs in the prediction of temperature and moisture tendencies (e.g., Das *et al.* 1999, Randall *et al.* 2003a, Xie *et al.* 2005). This result suggests that CRMs can be important tools for improving the representation of moist processes in GCMs.

At present, however, CRMs are not global models and can only simulate clouds and cloud systems over relatively small domains. In GCSS-style tests, the CRM results depend strongly on the quality of the input large-scale forcing, and it is difficult to separate model errors from observational forcing errors. Furthermore, offline CRM simulations with observed forcing allow only one-way interaction (large-scale to cloud-scale) and cannot

simulate the effects of cloud and radiation feedbacks on the large-scale circulation. Recently Grabowski and Smolarkiewicz (1999) and Khairoutdinov and Randall (2001) proposed a multi-scale modeling framework (MMF, sometimes termed a "*super-parameterization*"), which replaces the conventional cloud parameterizations with a CRM in each grid column of a GCM. The MMF can explicitly simulate deep convection, cloudiness and cloud overlap, cloud-radiation interaction, surface fluxes, and surface hydrology at the resolution of a CRM. It has global coverage, and allows two-way interactions between the CRMs and a GCM. An overview of this promising approach is given in Randall *et al.* (2003b) and Khairoutdinov *et al.* (2005). An MMF can be considered as a natural extension of the current SCM and CRM modeling activities of GCSS, NASA's Modeling Analyses and Modeling (MAP) program, the U.S. Department of Energy's Atmospheric Radiation Measurements (ARM) Program, and other programs devoted to improving cloud parameterizations in GCMs.

This paper describes the main characteristics of a new MMF developed at the Goddard Space Flight Center. The performance and applications of the Goddard MMF are analyzed for two different climate events, the 1998 El Nino and the 1999 La Nina. The differences and similarities between the Colorado State University (CSU) MMF (Khairoutdinov *et al.* 2005) and the Goddard MMF are summarized. Results from the Goddard MMF are compared with those from a GCM using conventional cloud parameterizations. In addition, some critical issues associated with the Goddard MMF are discussed.

2. Multi-scale Modeling System

The Goddard MMF is based the NASA Goddard finite-volume GCM (fvGCM) and the Goddard Cumulus Ensemble model (GCE, a CRM). The fvGCM provides global coverage while the GCE allows for the explicit simulation of cloud processes and their interactions with radiation and surface processes. This coupled modeling system allows cloud processes to be simulated on a variety of scales. The main characteristics of the fvGCM, GCE and Goddard MMF are briefly summarized in this section.

2.1 fvGCM

The fvGCM has been constructed by combining the finite-volume dynamic core developed at Goddard (Lin 2004) with the physics package of the NCAR Community Climate Model CCM3, which represents a well-balanced set of processes with a long history of development and documentation (Kiehl *et al.* 1998). The unique features of the finite-volume dynamical core include: an accurate conservative flux-form semi-Lagrangian transport algorithm (FFSL) with a monotonicity constraint on sub-grid distributions that is free of Gibbs oscillation (Lin and Rood 1996, 1997), a terrain-following Lagrangian control-volume vertical coordinate, a physically consistent integration of the pressure gradient force for a terrain-following coordinate (Lin 1997), and a mass-, momentum-, and total-energy-conserving vertical remapping algorithm. The physical parameterizations of the fvGCM have been upgraded by incorporating the gravity-wave drag scheme of the NCAR Whole Atmosphere Community Model (WACCM) and the Community Land Model version 2 (CLM-2; Bonan *et al*. 2002). This model has been applied in climate simulation, data

assimilation and prediction modes (Atlas *et al.* 2005, Shen *et al.* 2006a,b). Depending upon the application, the number of levels varies between 32 and 64, while the horizontal grid spacing varies between 2.5^{o} and 0.125^{o}.

2.2 GCE model

The GCE model has been developed and improved at Goddard Space Flight Center over the past two decades. The development and main features of the GCE were published in Tao and Simpson (1993) and Tao *et al.* (2003). A review of the applications of the GCE to developing a better understanding of precipitation processes can be found in Simpson and Tao (1993) and Tao (2003). The 3D version of the GCE is typically run using 256 x 256 up to 1024 x 1024 horizontal grid points at 1-2 km resolution or better.

A Kessler-type two-category liquid water (cloud water and rain) microphysical formulation is used with a choice of two three-class ice formulations (3ICE), namely that of Lin *et al*. (1983) and the Lin scheme modified to adopt slower graupel fall speeds as reported by Rutledge and Hobbs (1984). The sedimentation of falling ice crystals was recently included in the GCE scheme based on Heymsfield and Donner (1990) and Heymsfield and Iaquinta (2000), as discussed in detail in Hong *et al.* (2004). Two detailed, spectral-bin models (Khain *et al.* 1999, 2000; Chen and Lamb 1999) have also been implemented into the GCE. Atmospheric aerosols are included using number density size-distribution functions. The explicit spectral-bin microphysics can be used to study cloud-aerosol interactions and nucleation scavenging of aerosols as well as the impact of different concentrations and size

distributions of aerosol particles upon cloud formation (Fan *et al.* 2006; Li *et al.* 2006). These new microphysical schemes require the multi-dimensional Positive Definite Advection Transport Algorithm (MPDATA, Smolarkiewicz and Grabowski 1990) to avoid "decoupling" between mass and number concentration. Solar and infrared radiative transfer processes and their explicit interactions with clouds and the generation of subgrid-scale kinetic energy for both dry and moist processes are considered.

A sophisticated land surface modeling software package known as the Land Information System (LIS; Kumar *et al.* 2006) has recently been coupled with the GCE. LIS consists of an ensemble of land surface models (LSMs), including the Community Land Model, (CLM; Bonan *et al.* 2002); the community Noah LSM (Noah; Ek *et al.* 2003), and the Variable Infiltration Capacity model (VIC; Liang *et al.* 1996), among others. LIS is capable of being run in two modes: (i) fully coupled or “forecast” mode, where all meteorological inputs come from an atmospheric model such as GCE or WRF and (ii) uncoupled or “analysis” mode, where all meteorological inputs come from a combination of atmospheric analyses, satellite data and in situ station data. Because LIS can execute at horizontal spatial resolutions as fine as tens of meters--given that appropriate topography, soils, land cover and vegetation data is available--it is capable of resolving mesoscale features, including urban areas, lakes, and agricultural fields. This capability means that the impact and scaling of such heterogeneity on coupled cloud modeling can be studied. High-resolution GCE-LIS simulations (Zeng *et al.* 2006) indicate that the land surface can have an impact on cloud and precipitation processes especially for less-organized convective clouds.

2.3 A Coupled fvGCM-GCE Modeling System

A prototype MMF has been developed at Goddard based on the fvGCM and 2D GCE. It includes the fvGCM run with 2.5^o x 2^o horizontal grid spacing with 32 layers from the surface to 0.4 hpa, and the 2D (x-z) GCE using 64 horizontal grids (in the east-west orientation) and 32 levels with 4 km horizontal grid spacing and cyclic lateral boundaries. The time step for the 2D GCE is 10 seconds, and the fvGCM-GCE coupling interval is one hour (which is the fvGCM physical time step) at this resolution.

Because the vertical coordinate of the fvGCM (a terrain-following coordinate) is different from that of the GCE (a z coordinate), vertical interpolations are needed in the coupling interface. To interpolate fields from the GCE to the fvGCM, an existing fvGCM finite-volume piecewise parabolic mapping (PPM) algorithm is used, which conserves the mass, momentum, and total energy. A new finite-volume PPM algorithm, which conserves mass, momentum and moist static energy in the z coordinate is being developed to interpolate fields from the fvGCM to the GCE.

Table 1 compares the main characteristics of the Goddard and CSU MMFs. More CRMs, more frequent updating of the radiative processes (i.e., every 3 minutes), and inline cloud statistics (every minute) in the Goddard MMF, all increase the computational requirements compared to the CSU MMF.

3. Results

3.1 Performance of the Goddard MMF

The Goddard MMF has been evaluated against observations at inter-annual, intra-seasonal, and diurnal time scales under two different climate scenarios, namely, the 1998 El Nino and the 1999 La Nina. The model was forced by the observed sea surface temperatures (SSTs), and the initial conditions came from the Goddard Earth Observing System Version-4 (GEOS-4, Bloom *et al.* 2005) re-analyses at 0000 UTC 1 November 1997 and 1998, respectively. Similar runs with the same initial conditions and SSTs were performed using the fvGCM with NCAR CCM3 physics. The moist parameterization in the fvGCM includes the Zhang and MacFarlane (1995) scheme for deep convection and the Hack (1994) scheme for shallow and middle-level convection processes. The cloud parameterization follows a simple diagnosed condensation parameterization, and the cloud fraction is diagnosed following Slingo (1987). Both models have the same horizontal and vertical resolution (2^o by 2.5^o in the horizontal and 32 layers in the vertical).

Figure 1 shows the geographical distribution of simulated precipitation for January and July 1998 from the MMF and fvGCM, along with the corresponding observations from the Tropical Rainfall Measurement Mission (TRMM, Simpson *et al.* 1988, 1996) Microwave Imager (TMI, Kummerow *et al.* 2001). In general, given the observed SST forcing, the observed patterns of monthly-mean precipitation can be realistically simulated by both the MMF and fvGCM for extra-tropical storm tracks and the Tropics. The shift in tropical precipitation to the central Pacific in January 1998 during the El Nino is well captured. The

Inter-Tropical Convergence Zone (ITCZ), the South Pacific Convergence Zone (SPCZ), and the South Atlantic Convergence Zone (SACZ) are also well reproduced. The MMF precipitation patterns and dry areas tend to be slightly more realistic than those of the fvGCM; in particular, the unrealistic double ITCZ simulated by the fvGCM for July 1998 is not present in the MMF.

There are apparent biases in the MMF however: monthly-mean precipitation averaged over the Tropics is about 30% (4-6%) more than the TRMM observations (fvGCM) in both winter and summer. The MMF precipitation in the western Pacific, eastern tropical Pacific, Bay of Bengal and western India Ocean is too active during summer; a similar phenomenon occurs in simulations with the CSU MMF and has been called the "*Great Red Spot*" by Khairoutdinov *et al.* (2005). It is remarkable that both MMFs exhibit the *Great Red Spot* problem despite the many differences in their GCM dynamical cores, CRM dynamics, microphysics parameterizations, radiation, turbulence, and coupling strategies (Table 1). Due to the nonlinear coupling between the GCM and the CRM, the physical cause(s) of the *Great Red Spot* is(are) very difficult to isolate and identify. The use of 2D CRMs with cyclic lateral boundary conditions, which do not allow deep convective systems to propagate to the neighboring GCM grid boxes, is believed to be one of the causes of the *Great Red Spot* (Khairoutdinov *et al.* 2005). The cyclic lateral boundary conditions could lead to an excessive local convective-wind-evaporation feedback and ultimately the *Great Red Spot* (Luo and Stephens 2006). However, Khairoutdinov *et al.* (2005) have demonstrated that the *Great Red Spot* can be eliminated with a 3D CRM (using a small

domain, 8 x 8 grid points), especially when convective momentum transport is included[1]. Their study suggests that dimensionality (2D vs 3D CRM) and sampling in one direction might be the cause of the *Great Red Spot.*

Vertical velocities simulated by the Goddard MMF are stronger, particularly over the *Great Red Spot* region, than those in the fvGCM. This may be another factor in producing the *Great Red Spot* and could also explain why there is more precipitation in the MMF than fvGCM. Furthermore, the compensating downward motion (through mass conservation) was also stronger and produced stronger warming and drying in the MMF. This could cause the MMF to simulate larger and more realistic non-raining regions.

Figure 2 shows probability distribution functions (PDFs) of ice water content (IWC) at 147 hPa based on Microwave Limb Sounder (MLS) retrievals for January 2005 and for the period August 2004 to July 2005 as well as hourly instantaneous values of IWC from the Goddard MMF for January 1998. The MLS-retrieved annual (red color bars) and January (dark blue color bars) PDFs are similar, implying that the PDF is not too sensitive to the time of year when the whole Tropics is considered. Moreover, the PDFs clearly illustrate the sensitivity limits of the MLS instrument, namely that the precision of the MLS retrievals dictate a lower limit on the IWC values that can be detected, roughly ~0.4 (mg m^{-3}) at this pressure level. The Goddard MMF values, on the other hand, exhibit nonzero values in this low IWC range (< 0.4 mg m^{-3}). In addition, the Goddard MMF has a lower percentage of

[1] Their results also showed that precipitation amount was very sensitive to convective momentum transport when the 3D CRM was used. One the other hand, the precipitation amount is

IWCs between 1 ~ 20 (mg m^{-3}) than does the MLS data. The large ICW range (> 25.0 mg m^{-3}) simulated by the Goddard MMF occurs mainly over continents or coasts except for in the central and eastern Pacific during January 1998. Large vertical cloud velocities associated with storms that developed over land and coastal areas may explain the larger IWCs [convective available potential energy (CAPE) is larger over land than ocean]. For January 1998, deep convective systems responding to the warm SSTs in the central and eastern Pacific could produce large amounts of ice aloft. Overall, the comparison between the Goddard MMF and MLS IWC values generally shows good agreement in terms of the shape of the distribution. Similar results can be found for July 1998 and January and July 1999 (not shown).

The Madden-Julian Oscillation (MJO, Madden and Julian 1972, 1994), also known as the 30-60 day wave, is one of the most prominent large-scale features of the tropical general circulation. While the MJO is evident in circulation fields throughout the Tropics (Madden and Julian 1972; Knutson and Weickmann 1987), it is typically characterized by deep convection originating over the Indian Ocean and subsequent eastward propagation into the Pacific Ocean. Figure 3 shows Hovmoller diagrams of the daily tropical precipitation rate averaged between 10ºS and 10ºN from the Global Precipitation Climatology Project (GPCP), the fvGCM and Goddard MMF for 1998 and 1999. Both the fvGCM and MMF realistically reproduce the El Nino-associated eastward shift in the broad envelope of convection from the western Pacific warm pool to the eastern Pacific during winter 1997 and spring 1998 and the westward shift after summer 1998. During the 1999 La Nina, the broad-scale deep

---

quite similar in the Goddard MMF with and without convective momentum transport.

convective rain remains over the western Pacific warm pool region. Overall, the MMF (fvGCM) tends to produce stronger (weaker) convection than observed. Superimposed on the broad inter-annual patterns, the MMF shows vigorous convection propagating eastward at 30-60-day time scales, similar to what is observed. In contrast, the fvGCM run only shows some westward-propagating convection signals; the eastward-propagating MJO signals are virtually nonexistent. These results are consistent with the earlier findings (e.g., Randall *et al*. 2003b*;* Grabowski 2003, 2004) that MMFs can more realistically simulate the tropical intra-seasonal oscillation than GCMs with conventional cloud parameterizations.

The diurnal cycle is a fundamental mode of atmospheric variability. Successful simulation of the diurnal variability of the hydrologic cycle and radiative energy budget provides a robust test of physical processes represented in atmospheric models (e.g., Slingo *et al.* 1987; Randall *et al.* 1991; Lin *et al.* 2000). Figure 4 shows the geographical distribution of the local solar time (LST) of the non-drizzle precipitation frequency maximum in winter (left panels) and summer (right panels) of 1998 as simulated by the Goddard MMF (top panels) and the fvGCM (middle panels). Satellite microwave rainfall retrievals from a 5-satellite constellation including the TRMM TMI, Special Sensor Microwave Imager (SSMI) from the Defense Meteorological Satellite Program (DMSP) F13, F14 and F15, and the Advanced Microwave Scanning Radiometer – Earth Observing System (AMSR-E) onboard the Aqua satellite are analyzed at 1-h intervals from 1998 to 2005 for comparison. The non-drizzle precipitation is defined as precipitation that occurs such that the 1-h averaged rain rate is larger than 1 mm/day (see Lin *et al.* 2006).

Satellite microwave rainfall retrievals in general show that precipitation occurs most frequently in the afternoon to early evening over the major continents such as South and North America, Australia, and west and central Europe, reflecting the dominant role played by direct solar heating of the land surface. Over open oceans, a predominant early morning maximum in rain frequency can be seen in satellite observations, consistent with earlier studies (see a review by Sui *et al.* 1997, 2006). The MMF is superior to the fvGCM in reproducing the correct timing of the late afternoon and early evening precipitation maximum over land and the early morning precipitation maximum over the oceans. The fvGCM, in contrast, produces a dominant morning maximum rain frequency over major continents. Additional and more detailed comparisons between the observed and MMF-simulated diurnal variation of radiation fluxes, clouds and precipitation under different large-scale weather patterns and different climate regimes will be published elsewhere.

3.2 Comparison of the Goddard and CSU MMFs

Despite differences in model dynamics, coupling interfaces and physics between the Goddard and CSU MMFs, both simulate more realistic and stronger MJOs than traditional GCMs. However, both MMFs also have similar model biases, such as the *Great Red Spot* problem and the over-prediction of total surface rainfall over ocean compared to observations and the parent GCM (Tables 2 and 3). All of the model runs (i.e., from the two GCMs and the two MMFs) overestimate global rainfall compared to satellite estimates for 1998 (El Nino) and 1999 (La Nina). However, the CCM and CSU MMF-simulated rainfall are in better agreement with satellite estimates than the fvGCM and Goddard MMF for both years.

All of the model runs show less variation in total rainfall compared to satellite estimates. It might be expected that the MMF-simulated rainfall would be close to that of its parent GCM because many of the physical processes (i.e., surface processes, radiation, and SST) in the MMF are still the same as in the GCM. In addition, the key coupling strategy or design of the MMF is not to allow the MMF's mean field to systematically "drift" away from the corresponding GCM fields. One interesting result is that the Goddard MMF simulated more rainfall (about 3%) than its parent GCM for both years. In contrast, the CSU MMF simulated less rainfall (about 1%) than its parent GCM.

Both MMFs overestimate oceanic rainfall (2-3%) compared to their parent GCMs and satellite estimates for both years (Table 3). The CSU MMF simulated less rainfall over land than its parent GCM. This is why the CSU MMF simulated less global rainfall than its parent GCM (Table 2). The Goddard MMF overestimates global rainfall because of its oceanic component. The CSU MMF simulated the same amount of oceanic rainfall in both 1998 and 1999, implying that the CSU MMF is more sensitive to its land processes than its oceanic processes. The Goddard MMF shows slightly more variation in rainfall over ocean than land between 1998 and 1999.

Since all of the models (i.e., fvGCM, CCM, Goddard and CSU MMFs) and the satellite observations show almost identical global high, middle and low cloud amounts for 1998 and 1999, only the cloud amounts for 1998 are shown in Table 4. Both of the MMFs exhibit much better agreement with International Satellite Cloud Climatology Project

(ISCCP) cloud amounts (especially high and low) than do the GCMs. The CSU MMF-simulated high cloud amount agrees best with the satellite estimate.

The MMF approach is extremely computer intensive and can produce immense data sets. In this paper, only the variables and features inherent in their parent GCMs are compared. A more detailed comparison between the two MMFs for longer simulations (i.e., 5-10 year integrations), including simulated cloud properties from their CRM components as well as their improvements and sensitivities (see section 4), will be conducted in a separate paper.

4. Issues and Future Research

Despite the apparent promise of the MMF, only limited long-term simulations have been carried out with the system due to computational resources. To fully understand the strengths and weakness of the MMF approach in climate modeling, more research is needed to systematically study these issues with either the MMF itself or with offline CRM simulations. The model results also need to be tested thoroughly and rigorously against satellite and ground-based observations.

In addition, there are still many critical issues related to the MMF that may have a major impact on MMF performance. Specifically, the configuration of the CRMs within the MMF and the assumptions/physics used in the CRMs need to be addressed.

4.1 Configuration of CRMs within the MMF

Current MMF studies have only used 2D CRMs with cyclic lateral boundary conditions as proposed by Grabowski and Smolarkiewicz (1999) and Grabowski (2001). The potential weaknesses of the current framework are: **(1)** use of cyclic lateral boundary conditions in the CRM, **(2)** CRMs in neighboring GCM grid boxes can communicate only through the GCM, **(3)** the use of simple approaches for communication between the GCM and the CRMs, **(4)** use of coarse vertical and horizontal grid sizes in the CRM (4 km for the latter in the present study), **(5)** the absence of land surface and terrain effects in the CRMs, **(6)** the two-dimensionality of the CRMs, **(7)** each CRM converges to a 1D cloud model as the GCM grid size approaches that of the CRM, **(8)** the use of one single type of bulk microphysics (i.e., a 3ice scheme with graupel as the third class of ice) and parameterizations for radiation and sub-grid-scale turbulent processes in the CRM, and **(9)** momentum feedbacks/interactions between the CRMs and GCM are not accounted for. Problems (1)-(3) have been recognized and studied by Grabowski (2001, 2004) and Jung and Arakawa (2005). Khairoutdinov and Randall (2001) tested the sensitivity of the CRM results to the domain geometry and horizontal grid size using an offline 2D CRM. Problems (6) and (7) could be addressed by the quasi-3D approach (Randall *et al.* 2003b; Arakawa 2004; see Fig. 5b). However, the quasi-3D approach is more difficult to implement and more expensive computationally. At Goddard, an MMF based on a global 2D CRM (see Fig. 5a) is also being developed to address issues (2) and (7). In addition to thermodynamic feedback, dynamic (momentum forcing) feedback is also needed.

4.2 Issues related to the CRM used in the MMF

Some of the deficiencies in the current MMF are related to the dynamic and physical processes used in the CRM. These issues can be studied either by using the MMF itself or through the use of offline 2D and/or 3D CRMs.

4.2.1 Dimensionality (2D vs 3D)

Real clouds and cloud systems are 3D. Because of the limitations of computer resources, a 2D CRM is being used in the MMF. Previous modeling studies indicated that (e.g., Tao and Soong 1986; Lipps and Hemler 1986; Tao *et al*. 1987) the collective thermodynamic feedback effect and the vertical transports of mass, sensible heat, and moisture were quite similar between 2D and 3D numerical simulations. The fractional cloud coverage between the 2D and 3D simulations, however, differed between 2% (in the lower troposphere) and 10% (between 300 and 400 mb) in the cases studied. In these 3D simulations, the model domain was small and integration times were between 3 and 6 hours. However, Grabowski *et al.* (1998) found that cloud statistics as well as surface precipitation were significantly different for their 2D and 3D simulations if cloud radiation was fully interactive over their 7-day integrations. Zeng *et al.* (2006) found that the 3D-simulated surface rainfall is in better agreement with observations than its 2D for two ARM cases. They also found that the momentum field is quite similar between 2D and 3D simulations when both models are

nudged with the same large-scale observed winds at 1, 6, 12 and 24 hour model integration times.

Only thermodynamic feedback is allowed in the current Goddard and CSU MMFs, although Khairoutdinov *et al.* (2005) did perform some tests using a 3D CRM with momentum feedback. The 2D CRM orientation in the Goddard MMF is east-west. The CSU MMF has been run with both east-west and north-south orientations, and the north-south orientation has been adopted in a recent study (Khairoutdinov and Randall 2006). The fractional cloudiness and mesoscale organization are mainly determined by the vertical shear of the low-level wind. The surface fluxes also depend on the near-surface wind. Offline tests comparing 2D CRM simulations using east-west and south-north configurations are needed. The similarities and differences between 2D (east-west and south-north) and 3D for both short and long-term integration and in both active and inactive convective periods need to be identified.

4.2.2 Anelastic vs Compressible

The CRM dynamics can be either anelastic (Ogura and Phillips 1962), filtering out sound waves, or compressible (Klemp and Wilhelmson 1978), allowing sound waves. The sound waves are not important for thermal convection, but because of their high propagation speed, they create severe restrictions on the time step used in numerical integrations. For this reason, most cloud models (including those used in the Goddard and CSU MMFs) use an anelastic system of equations in which sound waves have been filtered. One advantage of

the compressible system is its computational simplicity and flexibility. Sensitivity tests are needed to examine the impact of compressibility on the MMF results.

4.2.3 Grid Size (Vertical and Horizontal)

For CRMs, the choice of horizontal and vertical grid spacing is an important issue and can have a major impact on the resolved convective processes. For example, Tompkins and Emanuel (2000) suggested that high vertical resolution (finer than 33 hPa) is needed to simulate realistic water vapor profiles and stratiform precipitation processes. In addition, much finer resolution is required for simulating realistic stratocumulus (Dr. Bjorn Stevens, personal communication). A comprehensive study of the sensitivity of various cloud types and/or systems to vertical and horizontal grid resolution is needed. The results from offline CRM research can help to determine the grid size requirements for the CRMs used in MMFs.

4.2.4 Microphysics

Both the Goddard and CSU MMF use a single one-moment bulk microphysical scheme (e.g., the 3ICE scheme with graupel) for all clouds and cloud systems. Typically, graupel with its low density and a high intercept (i.e., high number concentration) is used as the third class of ice when simulating tropical oceanic systems. In contrast, hail has a high density, small intercept, and fast fall speed and is used to simulate midlatitude continental systems (McCumber *et al.* 1991; Tao *et al.* 1996). Therefore, sensitivity tests are required to examine the impact of different bulk microphysical schemes (e.g., 3ICE with graupel, 3ICE with hail)

in the MMF. By comparing model results with observations, errors in the simulated hydrometeor fields can be investigated, identified and documented, especially in regards to uncertainties often associated with the cloud microphysical schemes. The effects of aerosols should also be tested with advanced microphysical schemes (i.e., spectral bin microphysics or a multi-moment scheme).

4.2.5 Land Surface

Interactions between the atmosphere and the land surface have considerable influence on local, regional and global climate variability. Therefore, coupled land-atmosphere systems that can realistically represent these interactions are critical for improving our understanding of the atmosphere-biosphere exchanges of water, energy, and their associated feedbacks. By coupling a high-resolution land surface modeling system (i.e., LIS) into the MMF, the interaction between soil, vegetation, and precipitation processes can be studied. As only 2D CRMs are being used in the MMF, how to specify the observed heterogeneities of land characteristics in 2D (with cyclic lateral boundary conditions) could be a major issue. Therefore, a method to allow heterogeneous surface processes (surface fluxes and/or land characteristics) in the coupled CRM-LIS system needs to be developed. The simplest method is a random distribution (Zeng *et al.* 2006). A more physical approach could use PDF matching between observed surface fluxes (or land characteristics) and modeled surface properties (i.e., the product of wind stress and air-land temperature/moisture differences, or rainfall). Both methods will be tested to improve the MMF's ability to represent these processes and to identify the key land-atmosphere feedbacks and their impact on the local

and regional water and energy cycles.

5. Summary

The idea for the MMF, whereby conventional cloud parameterizations are replaced with CRMs in each grid column of a GCM, was proposed by Grabowski and Smolarkiewicz (1999). Khairoutdinov and Randall (2001) and Randall *et al.* (2003b) developed the first MMF based on a GCM developed at NCAR (CAM) and a CRM at CSU. A second, more recent MMF based on the fvGCM and the GCE has been developed. This Goddard MMF's performance was evaluated and compared against satellite observations, its parent GCM (fvGCM) and the CSU MMF. The major highlights are as follows:

o The MMF-simulated surface precipitation pattern agrees with TRMM estimates, especially in the non-rainy region. Compensating downward motion away from major precipitation centers was stronger and produced stronger warming and drying in the MMF. This could lead the MMF to simulate larger and more realistic non-raining regions.

o The comparison between the MMF and MLS IWCs generally shows good agreement in terms of the shape of the distribution. However, the MLS did not detect the small (between 0.1 – 0.4 mg/m^3) and large IWCs (> 4 mg/m^3) that were simulated in the MMF.

o The MMF-simulated diurnal variation of precipitation shows good agreement with merged microwave observations. For example, the MMF-simulated frequency maximum was in the late afternoon (1400-1800 LST) over land and in the early morning (0500-0700 LST) over the oceans. The fvGCM-simulated frequency maximum was too early for both oceans and land.

o The MMF-simulated MJO shows vigorous eastward propagation at 30-60-day time scales, similar to what is observed. In contrast, the fvGCM-simulated MJO is very weak and the observed eastward-propagating MJO signals are nonexistent.

o Despite differences in model dynamics, coupling interfaces and physics between the Goddard and CSU MMFs, they both performed better against observations than did their parent GCMs. However, both MMFs also simulated the *Great Red Spot* (i.e., an over estimation of precipitation in the western Pacific). The *Great Red Spot* problem could be due to the cyclic lateral boundary conditions, the two-dimensionality of the CRMs, localized convective-wind–evaporation feedback, stronger vertical upward motion or a combination of factors. There are also differences between the two MMFs. For example, the CSU MMF simulated less rainfall over land than its parent GCM. This is why the CSU MMF simulated less global rainfall than its parent GCM. The Goddard MMF, however, overestimates global rainfall because of its oceanic component.

o Comparisons between the two MMFs for 1998 and 1999 were based on variables from their parent GCMs. A more detailed comparison between the two MMFs for longer

simulations (i.e., 5-10 years integration), including simulated cloud properties from their CRM components, is needed.

o A better design for future MMFs is needed and being developed (i.e, quasi-3D and global 2D). Since the embedded CRMs allow for the explicit simulation of cloud processes and their interaction with radiation and surface processes, the CRM's own dynamic and physical processes could cause deficiencies in the current MMF. Major CRM-related issues were discussed in detail (Section 4).

MMFs can bridge the gap between traditional CRM simulations that have been applied over the past two decades and future non-hydrostatic high-resolution global CRMs. The traditional CRM needs large-scale advective forcing in temperature and water vapor from intensive sounding networks deployed during major field experiments or from large-scale model analyses to be imposed as an external forcing (Soong and Ogura 1980; Soong and Tao 1980; Tao and Soong 1986; Krueger *et al.* 1988; and many others). A weakness of this approach is that the simulated rainfall, temperature and water vapor budget are forced to be in good agreement with observations (see Tao 2003 for a brief review; and Randall *et al.* 2003a). However, there is no feedback from the CRM to the large-scale model (i.e., the CRM environment). In contrast, an MMF allows explicit interactions between the CRM and the GCM. Traditional CRMs can only examine the sensitivity of model grid size or physics for one type of cloud/cloud system at a single geographic location. MMFs, however, could be used to identify the optimal grid size and physical processes (i.e., microphysics, cloud-radiation interaction) on a global scale.

6. Acknowledgements

The authors thank Dr. D. Anderson for his support for developing the MMF under the NASA IDS and Cloud Modeling and Analysis Initiative (CMAI) program. The GCE is mainly supported by the NASA Headquarters Atmospheric Dynamics and Thermodynamics Program and TRMM. The first author and J. Simpson are grateful to Dr. R. Kakar at NASA headquarters for his support of GCE development over the past decade. The authors also thank Mr. S. Lang and Dr. D. Starr for proof reading and providing comments, respectively.

Acknowledgment is also made to the NASA Goddard Space Flight Center and Ames Center for computer time used in this research.

7. References

Arakawa, A., 2004: The cumulus parameterization problem: Past, present, and future. *J. Climate*, **17**, 2493-2525.

Atlas, R., O. Reale, B.-W. Shen, S.-J. Lin, J.-D. Chern, W. Putman, T. Lee, K.-S. Yeh, M. Bosilovich, and J. Radakovich, 2005: Hurricane forecasting with the high-resolution NASA finite-volume General Circulation Model, *Geophysical Research Letters*, **32**, L03801, doi:10.1029/2004GL021513.

Bloom, S., A. da Silva, D. Dee, M. Bosilovich, J.-D. Chern, S. Pawson, S. Schubert, M. Sienkiewicz, I. Stajner, W.-W. Tan, M.-L. Wu, 2005: Documentation and Validation of the Goddard Earth Observing System (GEOS) Data Assimilation System - Version 4. Technical Report Series on Global Modeling and Data Assimilation 104606, **26**.

Bonan, G. B., K. W. Oleson, M. Vertenstein, S. Levis, X. Zeng, Y. Dai, R. E. Dickinson, and Z.-L. Yang, 2002: The Land Surface Climatology of the Community Land Model Coupled to the NCAR Community Climate Model. *J. Clim*, **15**(22), 3123–3149.

Chen, J-.P., and D. Lamb, 1999: Simulation of cloud microphysical and chemical processes using a multicomponent framework. Part II: Microphysical evolution of a wintertime orographic cloud. *J. Atmos. Sci.*, **56**, 2293-2312.

Das, S., D. Johnson and W.-K. Tao, 1999: Single-column and cloud ensemble model simulations of TOGA COARE convective systems, *J. Meteor. Soc. Japan*, **77**, 803-826.

DeMott, C. A., D. A. Randall, and M. Lhairoutdinov, 2006: Convective precipitation variability as a tool for general circulation model analysis. *J. Climate*, (accepted).

Ek, M. B., K. E. Mitchell, Y. Lin, E. Rogers, P. Grunmann, V. Koren, G. Gayno, and J. D. Tarpley, 2003: Implementation of Noah land surface model advances in the National Centers for Environmental Prediction operational mesoscale Eta model, *J. Geophys. Res.*, **108**(D22), 8851, doi:10.1029/2002JD003296.

Fan, J., R. Zhang, G. Li, W.-K. Tao, X. Li, 2006: Simulations of cumulus clouds using a spectral bin microphysics in a cloud resolving model. *J. Geophy. Res*., (in press).

GEWEX Cloud System Study (GCSS), 1993: *Bull. Amer. Meteor. Soc.*, **74**, 387-400.

Grabowski, W. W., X. Wu, and M. W. Moncrieff, and W. D. Hall, 1998: Cloud resolving modeling of tropical cloud systems during PHASE III of GATE. Part II: Effects of resolution and the third dimension. *J. Atmos. Sci.*, **55**, 3264-3282.

Grabowski, W. W., and P. K. Smolarkiewicz, 1999: CRCP: A cloud resolving convective parameterization for modeling the tropical convective atmosphere. *Physica*, **133**, 171-178.

Grabowski, W. W., 2001: Coupling cloud processes with the large scale dynamics using the cloud resolving convection parameterization (CRCP). *J. Atmos. Sci*., **58**, 978-997.

Grabowski, W. W., 2003: MJO-like coherent structures: Sensitivity simulations using the cloud-resolving convection parameterization (CRCP). *J. Atmos. Sci.*, **60**, 847-864.

Grabowski, W. W., 2004: An improved framework for superparameterization. *J. Atmos. Sci.*, **61**, 1940-1952.

Hack, J. J., 1994: Parameterization of moist convection in the National Center for Atmospheric Research community climate model (CCM2), *J. Geophys. Res.*, **99** (D3), 5551-5568.

Heymsfield, A. J., and L. J. Donner, 1990: A scheme for parameterizing ice-cloud water content in general circulation models. *J. Atmos. Sci.*, **47**, 1865-1877.

Heymsfield, A. J., and J. Iaquinta, 2000: Cirrus crystal terminal velocities. *J. Atmos. Sci.*, **57**, 916-938.

Hong, S.-Y., J. Dudhia, and S.-H. Chen, 2004: A revised approach to ice-microphysical processes for the bulk parameterization of cloud and precipitation. *Mon. Wea. Rev.*, **132**, 103–120.

Jung, J.-H., and A. Arakawa, 2005: Preliminary tests of multiscale modeling with a two-dimensional framework: Sensitivity to coupling methods. *Mon. Wea. Rev*., **133**, 649-662.

Khain, A. P., A. Pokrovsky, and I. Sednev, 1999: Some effects of cloud-aerosol interaction on cloud microphysics structure and precipitation formation: Numerical experiments with a spectral microphysics cloud ensemble model. *Atmos. Res.*, **52**, 195-220.

Khain, A. P., M. Ovtchinnikov, M. Pinsky, A. Pokrovsky, and H. Krugliak, 2000: Notes on the state-of-the-art numerical modeling of cloud microphysics. *Atmos. Res*., **55**, 159-224.

Khairoutdinov, M. F., and D. A. Randall, 2001: A cloud resolving model as a cloud parameterization in the NCAR community climate system model: Preli-minary results. *Geophys. Res. Lett*., **28**, 3617-3620.

Khairoutdinov, M. F., and D. A. Randall, 2003: Cloud resolving modeling of the ARM Summer1997 IOP: Model formulation, results, uncertainties, and sensitivities. *J. Atmos. Sci.,* **60**, 607-625.

Khairoutdinov, M. F., D. A. Randall, and C DeMott, 2005: Simulations of the Atmospheric General Circulation Using a Cloud-Resolving Model as a Superparameterization of Physical Processes. *J. Atmos. Sci.*, **62**, 2136-2154.

Khairoutdinov, M. F., and D. A. Randall, 2006: Evaluation of the simulated interannual and subseasonal variability in an AMIP-style simulation using the CSU Multiscale Modeling Framework. *J. Climate*, (submitted).

Kiehl,J. T., J. J. Hack, G. B. Bonan, B. A. Boville, D. L. Williamson, and P. J. Rasch, 1998: The National Center for Atmospheric Research Community Climate Model: CCM3. *J. Climate*, **11**, 1131–1150.

Klemp, J. B., and R. Wilhelmson, 1978: The simulation of three-dimensional convective storm dynamics. *J. Atmos. Sci.*, **35**, 1070-1096.

Krueger, S.K., 1988: Numerical simulation of tropical cumulus clouds and their interaction with the subcloud layer. *J. Atmos. Sci.*, **45**, 2221-2250.

Knutson, T. R., and K. M. Weickmann, 1987: 30-60 day atmospheric oscillations: Composite life cycles of convection and circulation anomalies. *Mon. Wea. Rev*., **115**, 1407-1436.

Kumar, S. V., C. D. Peters-Lidard, Y. Tian, P. R. Houser, J. Geiger, S. Olden, L. Lighty, J. L. Eastman, B. Doty, P. Dirmeyer, J. Adams, K. Mitchell, E. F. Wood and J. Sheffield, 2006: Land Information System - An Interoperable Framework for High Resolution Land Surface Modeling. *Environmental Modeling & Software*, **21**, 1402-1415.

Kummerow, C., Y. Hong, W.S. Olson, S. Yang, R.F. Adler, J. McCollum, R. Ferraro, G. Petty, D.-B. Shin, and T.T. Wilheit, 2001: The evolution of the Goddard profile algorithm (GPROF) for rainfall estimation from passive microwave sensors. *J. Appl. Meteor.*, **40**, 1801-1820.

Li, X., W.-K. Tao, A. Khain, J. Simpson and D. Johnson, 2006: Sensitivity of (bulk vs explicit-bin) microphysics in cloud-resolving model simulated mid-latitude squall line: Part I: Model validation. *J. Atmos. Sci*., (submitted).

Liang, X, E. F. Wood, and D. P. Lettenmaier, 1996: Surface soil moisture parameterization of the VIC-2L model: Evaluation and modification. *Global and Planetary Change*. **13**(1-4), 195-206.

Lin, S.-J., 2004: A "vertically Lagrangian" finite-volume dynamical core for global models. *Mon. Wea. Rev.*, **32**, 2293-2307.

Lin, S.-J., 1997: A finite-volume integration method for computing pressure gradient forces in general vertical coordinates. *Q. J. Roy. Met. Soc.*, **123**, 1749-1762.

Lin, S.-J., and R. B. Rood, 1997: An explicit flux-form semi-Lagrangian shallow water model on the sphere. *Q. J. Roy. Met. Soc.*, **123**, 2477-2498.

Lin, S.-J., and R. B. Rood, 1996: Multidimensional flux-form semi-Lagrangian transport schemes. *Mon. Wea. Rev.*, **124**, 2046-2070.

Lin, X., D. A. Randall, and L. D. Fowler, 2000: Diurnal variability of the hydrological cycle and radiative fluxes: Comparisons between observations and a GCM. *J. Climate*, **13**, 4159-4179.

Lin, X., S. Zhang, and A. Y. Hou, 2006: Variational assimilation of global microwave rainfall retrievals: Physical and dynamical impact on GEOS analyses. Conditionally *Mon. Wea. Rev*., (accepted).

Lin, Y.-L., R. D. Farley, and H. D. Orville, 1983: Bulk parameterization of the snow field in a cloud model. *J. Clim.ate Appl. Meteor.*, **22**, 1065-1092.

Lipps, F. B., and R. S. Helmer, 1986: Numerical simulation of deep tropical convection associated with large-scale convergence. *J. Atmos. Sci.*, **43**, 1796-1816.

Luo, Z., and G. L. Stephens, 2006: An enhanced convection-wind-evaporation feedback in a superparameterization GCM (SP-GCM) depiction of the Asian summer monsoon. *J. Geophys. Lett*., **33**, L06707, doi:10.1029/2005GL025060.

Madden, R. A., and P. R. Julian, 1972: Description of global-scale circulation cells in the Tropics with a 40-50 day period. *J. Atmos. Sci*., **29**, 1109-1123.

Madden, R. A., and P. R. Julian, 1994: Observations of the 40-50-day tropical oscillation—A review. *Mon. Wea. Rev.*, **122**, 814-837.

McCumber, M., W.-K. Tao, J. Simpson, R. Penc, and S.-T. Soong, 1991: Comparison of ice-phase microphysical parameterization schemes using numerical simulations of convection. *J. Appl. Meteor*., **30**, 987-1004.

Ogura, Y., and N. A. Phillips, 1962: Scale analysis of deep and shallow convection in the atmosphere. *J. Atmos. Sci.*, **19**, 173-179.

Pincus, R., H. W. Baker, and J.-J. Mocrette, 2003: A fast, flexible, approximation technique fro computing radiative transfer in inhomogeneous cloud fields. *J. Geophys. Res*., **108 (D13)**, 4376,doi:10.1029/2002JD003322.

Randall, D.A., Harshvardhan, and D.A. Dazlich, 1991: Diurnal variability of the hydrologic cycle in a general circulation model. *J. Atmos. Sci*., **48**, 40-62.

Randall, D., S. Krueger, C. Bretherton, J. Curry, P. Duynkerke, M. Moncrieff, B. Ryan, D. Starr, M. Miller, W. Rossow, G. Tselioudis and B. Wielicki, 2003a: Confronting Models with Data: The GEWEX Cloud Systems Study. *Bull. Amer. Meteor. Soc.*, **84**, 455-469.

Randall, D., M. Khairoutdinov, A. Arakawa, and W. Grabowski, 2003b: Breaking the cloud parameteriza-tion deadlock. *Bull. Amer. Meteor. Soc*., **84**, 1547-1564.

Rutledge, S. A., and P. V. Hobbs, 1984: The mesoscale and microscale structure and organization of clouds and precipitation in mid-latitude clouds. Part XII: A diagnostic modeling study of precipitation development in narrow cold frontal rainbands. *J. Atmos. Sci.*, **41**, 2949-2972.

Shen, B.-W., R. Atlas, J.-D. Chern, O. Reale, S.-J. Lin, T. Lee, and J. Change 2006a: The Finite Volume General Mesoscale Circulation Model: Preliminary simulations of mesoscale vortices at 1/8 degree resolution. *Geophys. Res. Lett*., **33**, L05801, doi:10.1029/2005GL024594.

Shen, B.-W., R. Atlas, O. Oreale, S.-J Lin, J.-D. Chern, J. Chang, C. Henze, and J.-L. Li, 2006b: Hurricane Forecasts with a Global Mesoscale-Resolving Model: Preliminary Results with Hurricane Katrina (2005). *Geophys. Res. Lett*., 2006GL026143, in press.

Simpson, J., and W.-K. Tao, 1993: The Goddard Cumulus Ensemble Model. Part II: Applications for studying cloud precipitating processes and for NASA TRMM. *Terrestrial, Atmospheric and Oceanic Sciences (TAO)*, **4,** 73-116.

Simpson, J., R.F. Adler, and G. North, 1988: A Proposed Tropical Rainfall Measuring Mission (TRMM) satellite. *Bull. Amer. Meteor. Soc.*, **69**, 278-295.

Simpson, J., C. Kummerow, W.-K. Tao, and R. Adler, 1996: On the Tropical Rainfall Measuring Mission (TRMM), *Meteor. and Atmos. Phys.*, **60**, 19-36, 1996.

Slingo, J. M., 1987: The development and verification of a cloud prediction model for the ECMWF model. *Q. J. R. Met. Soc.,* **113**, 889-927.

Slingo, A., R. C. Wilderspin, and S. J. Brentnall, 1987: Simulation of the diurnal cycle of outgoing longwave radiation with an atmospheric GCM. *Mon. Wea. Rev.,* **115,** 1451–1457.

Smolarkiewicz, P. K., and W.W. Grabowski, 1990: The multidimensional positive advection transport algorithm: nonoscillatory option. *J. Comput. Phys.*, **86**, 355-375.

Soong, S.-T., and Y. Ogura, 1980: Response of trade wind cumuli to large-scale processes. *J. Atmos. Sci*., **37**, 2035-2050.

Soong, S.-T., and W.-K. Tao, 1980: Response of deep tropical clouds to mesoscale processes. *J. Atmos. Sci*., **37**, 2016-2036.

Sui, C.-H., K.-M. Lau, Y. Takayabu, and D. Short, 1997: Diurnal variations in tropical oceanic cumulus convection during TOGA COARE. *J. Atmos. Sci*., **54**, 637-655.

Sui, C.-L., X. Li, K.-M. Lau, W.-K. Tao and M.-D. Chou, 2006: Convective-radiative-mixing processes in the Tropical Ocean-Atmosphere. *Recent Progress in Atmospheric Sciences with Applications to the Asia-Pacific Region*, World Scientific Publication (accepted).

Tao, W.-K., and S.-T. Soong, 1986: A study of the response of deep tropical clouds to mesoscale processes: Three-dimensional numerical experiments. *J. Atmos. Sci.*, **43**, 2653-2676.

Tao, W.-K., J. Simpson, and S.-T. Soong, 1987: Statistical properties of a cloud ensemble: A numerical study. *J. Atmos. Sci.*, **44**, 3175-3187.

Tao, W.-K., S. Lang, J. Simpson, C.-H. Sui and B. Ferrier and M.-D. Chou, 1996: Mechanisms of Cloud-radiation interaction in the tropics and midlatitudes. *J. Atmos. Sci.*, **53**, 2624-2651.

Tao, W.-K., and J. Simpson, 1993: The Goddard Cumulus Ensemble Model. Part I: Model description. *Terrestrial, Atmospheric and Oceanic Sciences (TAO)*, **4**, 19-54.

Tao, W.-K., 2003: Goddard Cumulus Ensemble (GCE) model: Application for understanding precipitation processes, *AMS Monographs - Cloud Systems, Hurricanes and TRMM*. 103-138.

Tao, W.-K., J. Simpson, D. Baker, S. Braun, D. Johnson, B. Ferrier, A. Khain, S. Lang, C.-L. Shie, D. Starr, C.-H. Sui, Y. Wang and P. Wetzel, 2003: Microphysics, Radiation and Surface Processes in a Non-hydrostatic Model, *Meteorology and Atmospheric Physics*, **82**, 97-137.

Tompkins, A. M., and K. A. Emaunel 2000: The vertical resolution sensitivity of simulated equilibrium temperature and water vapor profiles. *Q. J. R. Meteorol. Soc.*, **126**, 1219-1238.

Xie, S., M. H. Zhang, M. Branson, R. T. Cederwall, A. D. Del Genio, Z. A. Eitzen, S. J. Ghan, S. F. Iacobellis, K. L. Johnson, M. Khairoutdinov, S. A. Klein, S. K. Krueger, W. Lin, U. Lohmann, M. A. Miller, D. A. Randall, R. C. J. Somerville, Y. C. Sud, G. K. Walker, A. Wolf, X. Wu, K.-M. Xu, J. J. Yio, G. Zhang and J. Zhang, 2005: Simulations of midlatitude frontal clouds by single-column and cloud-resolving models during the Atmospheric Radiation Measurement March 2000 cloud intensive operational period. *J. Geophys. Res.*, **110**. D15S03, doi:10.1029/2004JD005119.

Zeng, X., W.-K. Tao, M. Zhang, S. Lang, C. Peters-Lidard, J. Simpson, S. Xie, S. Kumar, J. V. Geiger, C.-L. Shie, and J. L.. Eastman, 2006: Evaluation of long-term cloud-resolving modeling with observational cloud data. *J. Atmos. Sci.,* (**accepted**).

Zhang, G. J., 2002: Convective quasi-equilibrium in midlatitude continental environment and its effect on convective parameterization. *J. Geophys. Res.*, **107**, D14, doi: 10.1029/2001JD001005.

Zhang, G. J., and N. A. McFarlane, 1995: Sensitivity of climate simulations to the parameterization of cumulus convection in the Canadian Climate Centre general circulation model. *Atmos. Ocean*, **33**, 407-446.

TABLES

Table 1 Major characteristics of the MMFs developed at CSU and NASA Goddard.

Table 2 The total rainfall amount for 1998 and 1999 from the fvGCM, Goddard MMF, CCM and CSU MMF. The observed rainfall (GPCP V3) is also shown for comparison.

Table 3 Same as Table 2 except showing rainfall over ocean and land.

Table 4 High, middle and low cloud amounts simulated from the fvGCM, Goddard MMF, CCM and CSU MMF. Observed cloud amounts are shown for comparison.

FIGURES

Fig. 1 Monthly precipitation rate (mm/day) from the TMI (upper panels) at 0.5^{o} resolution, fvGCM (middle panels), and Goddard MMF (lower panels) for January 1998 (left panels) and July 1998 (right panels).

Fig. 2 Probability distribution of MLS ice water content (mg m^{-3}) at 147 hPa for January 2005 (dark blue bars) and for the period of August 2004 ~ July 2005 (red bars) and from instantaneous fvMMF model output for January 1998 (yellow bars).

Fig. 3 Hovmoller diagrams of tropical (averaged from 10^{0} S to 10^{0} N) daily precipitation rate for the GPCP (left panels), fvGCM (center panels), and MMF (right panels) from 1 November 1997 to 31 December 1998 (upper panels) and from 1 November 1998 to 31 December 1999 (lower panels).

Fig. 4 Geographical distribution of the LST for the non-drizzle precipitation frequency maximum in winter (left panels) and summer (right panels) 1998 as simulated with the Goddard MMF (upper panels) and fvGCM (middle panels) and observed by satellite from 1998-2005 (bottom panels). Blank regions indicate no precipitation. The MMF results are based on detailed 2D GCE model-simulated hourly rainfall output.

Fig. 5 **(a)** A global 2D CRM structure (single east-west orientation). Cyclic lateral boundary conditions are replaced by direct coupling of the CRMs in neighboring GCM cells**. (b)** A quasi-3D CRM structure (from Randall et al. 2003b). Two orthogonal high-resolution CRM grids are extended to the walls of the GCM grid cells. In both of these new approaches, the effects of topography may be required in the embedded CRM.

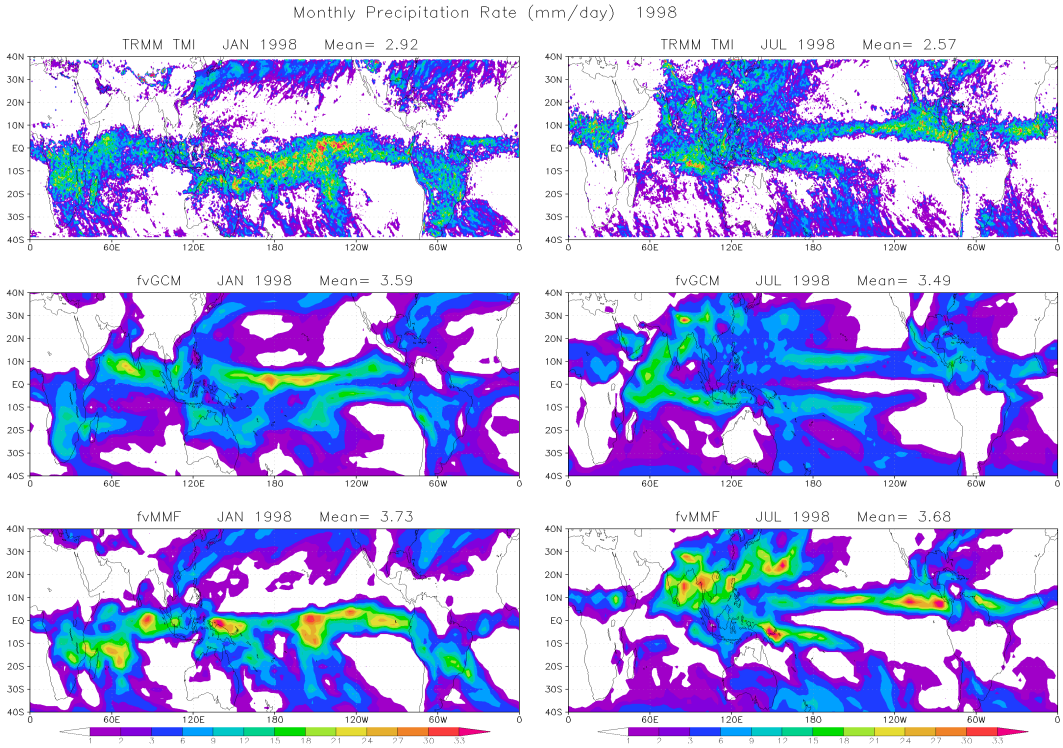

Fig. 1 *Monthly precipitation rate (mm/day) from the TMI (upper panels) at 0.5^o resolution, fvGCM (middle panels), and Goddard MMF (lower panels) for January 1998 (left panels) and July 1998 (right panels).*

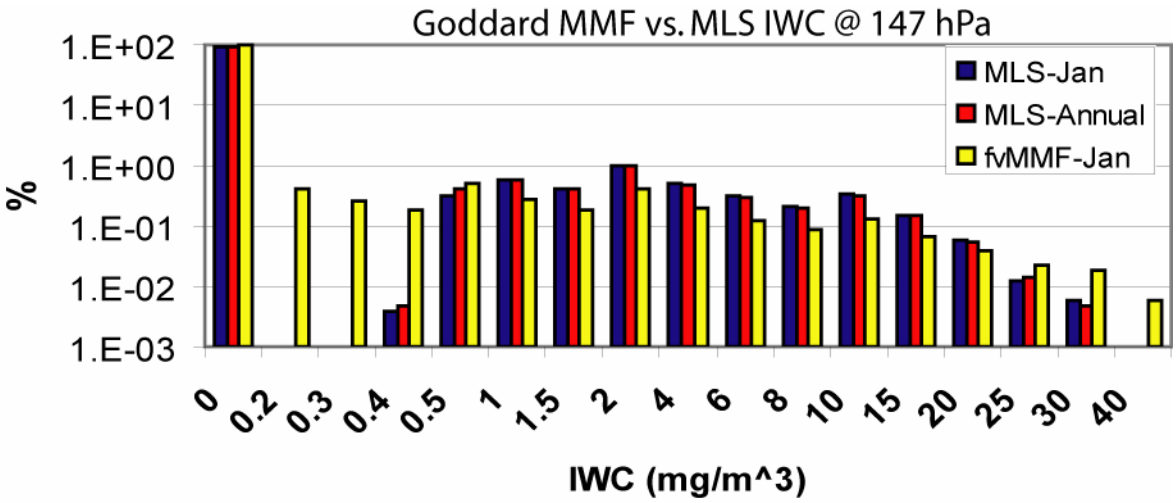

Fig. 2 *Probability distribution of MLS ice water content (mg m^{-3}) at 147 hPa for January 2005 (dark blue bars) and for the period August 2004 ~ July 2005 (red bars) and from instantaneous Goddard MMF output for January 1998 (yellow bars).*

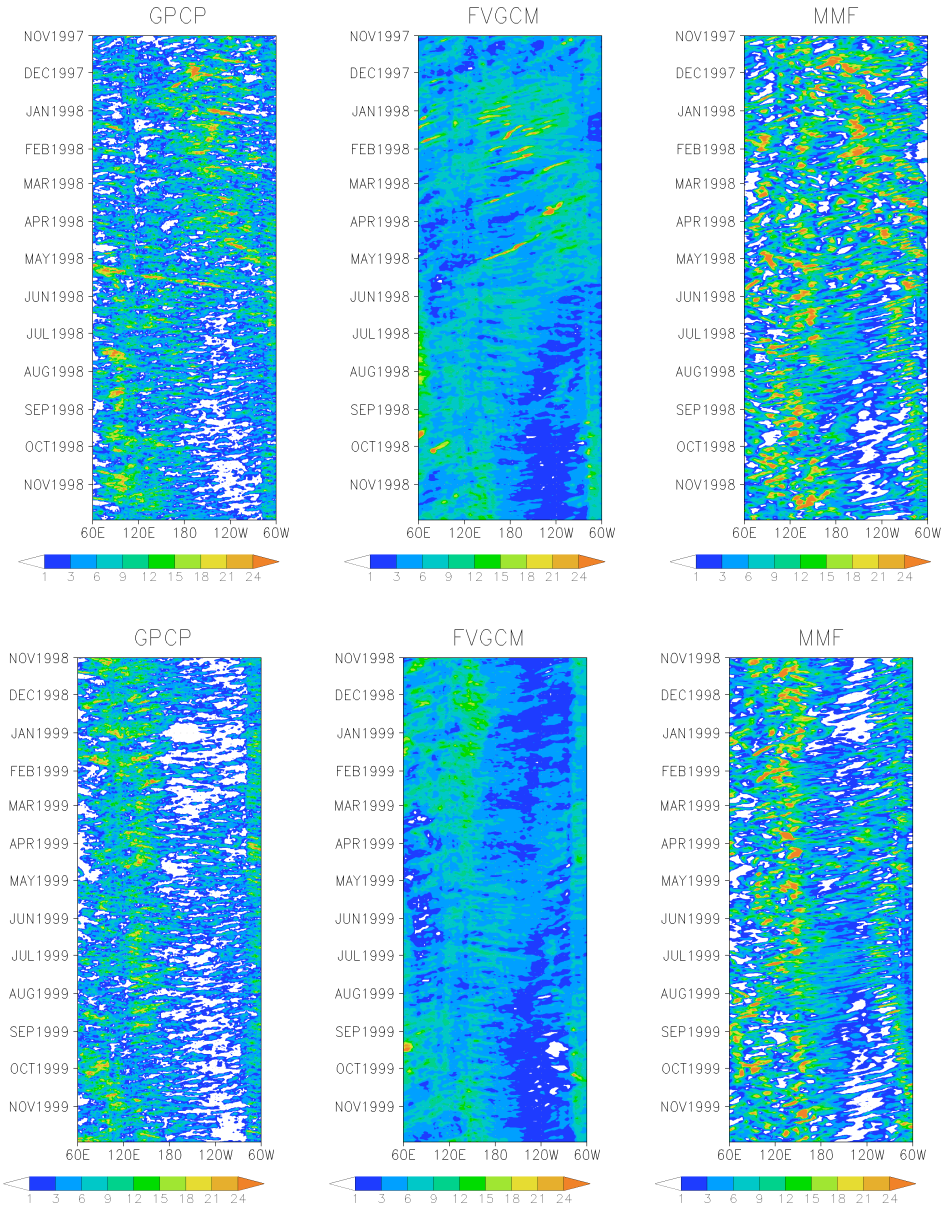

Fig. 3 Hovmoller diagrams of tropical (averaged from 10^0 S to 10^0 N) daily precipitation rate for the GPCP (left panels), fvGCM (center panels), and MMF (right panels) from 1 November 1997 to 31 December 1998 (upper panels) and from 1 November 1998 to 31 December 1999 (lower panels).

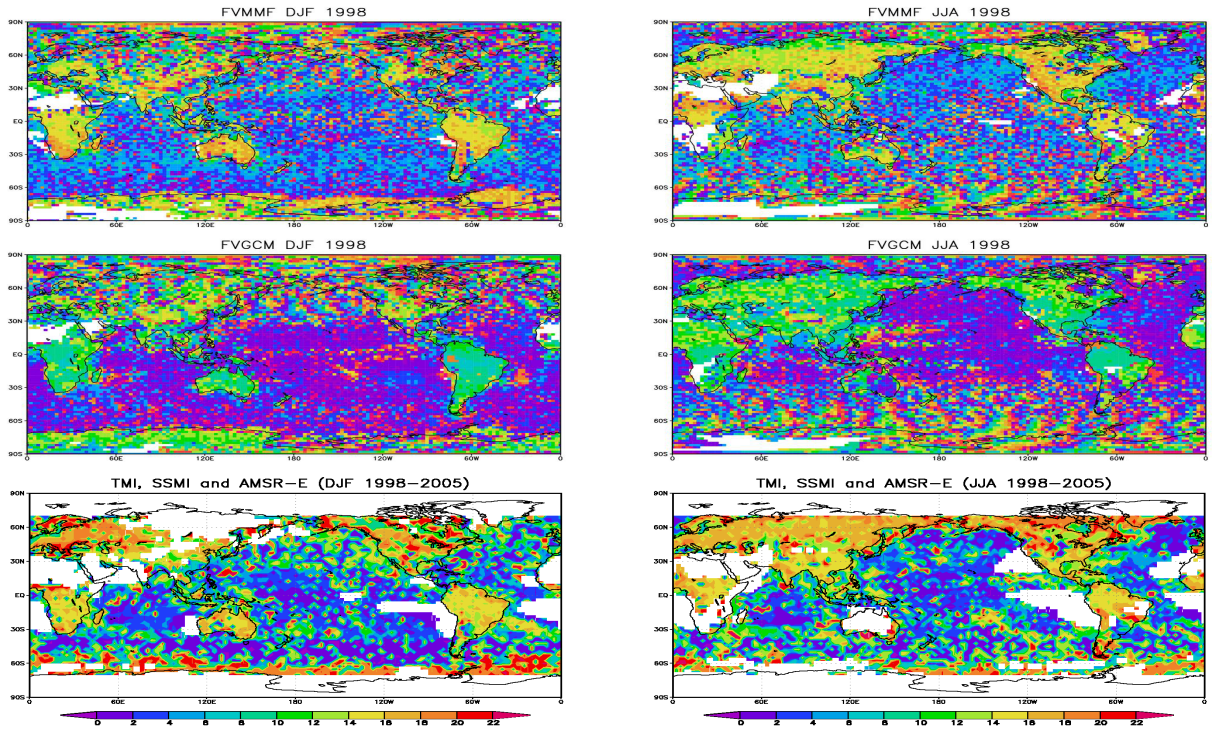

Fig. 4 Geographical distribution of the LST for the non-drizzle precipitation frequency maximum in winter (left panels) and summer (right panels) 1998 as simulated with the Goddard MMF (upper panels) and fvGCM (middle panels) and observed by satellite from 1998-2005 (bottom panels). Blank regions indicate no precipitation. The MMF results are based on detailed 2D GCE model-simulated hourly rainfall output.

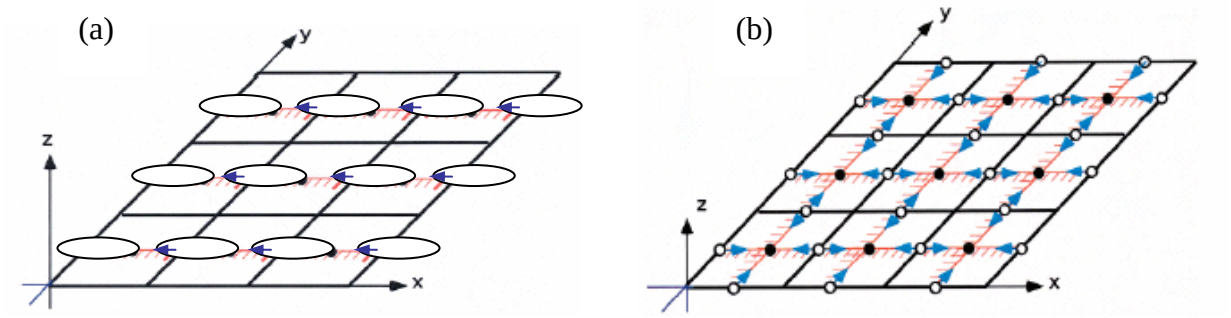

Fig. 5 ***(a)*** *A global 2D CRM structure (single east-west orientation). Cyclic lateral boundary conditions are replaced by direct coupling of the CRMs in neighboring GCM cells.* ***(b)*** *A quasi-3D CRM structure (from Randall et al. 2003b). Two orthogonal high-resolution CRM grids are extended to the walls of the GCM grid cells. In both of these new approaches, the effects of topography may be required in the embedded CRM.*

CSU MMF	NASA MMF
CCM-CSU/CRM	fvGCM – GCEM
T42 (8192 CRMs)	2 x 2.5 degree (12960 CRMs)
Microphysics (Khairoutdinov and Randall 2003) (~15 processes)	Three Microphysics Options (> 40 processes)
Positive definite advection scheme	Positive definite advection scheme
1.5 order TKE	1.5 order TKE
NCAR CCM3 Radiation (Blackmon *et al.* 2001) (every 15 min)	Goddard Radiation (every 3 min)
Time step (20 s)	Time step (10 s)
24 vertical layers	32 vertical layers (as fvGCM)
None	Inline cloud statistics (every 1 min)
In development	Land surface model (LIS)
43 hours/per simulated year on a 1024 CPU computer	278 hours/per simulated year on a 512 CPU computer

Table 1 Major characteristics of the MMFs developed at CSU and NASA Goddard.

	Observation	fvGCM	Goddard MMF	CCM	CSU MMF
1998	2.65	3.07	3.17	2.88	2.84
1999	2.59	3.05	3.14	2.83	2.81

Table 2 The total rainfall amount for 1998 and 1999 from the fvGCM, Goddard MMF, CCM and CSU MMF. The observed rainfall (GPCP V3) is also shown for comparison.

	Observation	**fvGCM**	**Goddard MMF**	**CCM**	**CSU MMF**
1998 (Ocean)	2.92	3.43	3.55	3.08	3.15
1998 (Land)	2.02	2.21	2.27	2.38	2.06
1999 (Ocean)	2.80	3.38	3.52	3.04	3.15
1999 (Land)	2.09	2.26	2.25	2.34	1.98

Table 3 Same as Table 2 except showing rainfall over ocean and land.

	Observation	**fvGCM**	**Goddard MMF**	**CCM**	**CSU MMF**
1998 High cloud amount	0.12	0.38	0.21	0.36	0.14
1998 Middle cloud amount	0.20	0.21	0.17	0.21	0.15
1998 Low cloud amount	0.27	0.45	0.35	0.43	0.33

Table 4 High, middle and low cloud amounts simulated from the fvGCM, Goddard MMF, CCM and CSU MMF. Observed cloud amounts are shown for comparison.